NMR in Biomedicine

Magnetization Transfer in Liposome and Proteoliposome Samples that Mimic the Protein and Lipid Composition of Myelin

Journal:	*NMR in Biomedicine*
Manuscript ID	NBM-18-0192.R2
Wiley - Manuscript type:	Research Article
Date Submitted by the Author:	n/a
Complete List of Authors:	Yang, Weiqi; Department of Chemistry, New York University Lee, Jae-Seung; Department of Chemistry, New York University; Department of Radiology, New York University Langone Medical Center Leninger, Maureen; Department of Chemistry, New York University Windschuh, Johannes; Department of Radiology, New York University Langone Medical Center Traaseth, Nathaniel; Department of Chemistry, New York University Jerschow, Alexej; Department of Chemistry, New York University
Keywords:	Magnetization transfer (MT) < Endogenous Contrast Methods < Methods and Engineering, Chemical exchange saturation transfer < Endogenous Contrast Methods < Methods and Engineering, White matter diseases < Neurological < Applications

A proteoliposome model system to mimic the white matter system was used to examine the roles of protein, cholesterol, cerebrosides, and sphingomyelin. Exchange parameters were determined from z-spectrum experiments and double-quantum filter experiments. We found that cerebrosides, produced the strongest exchange effects, and that these were even more pronounced than those found for proteins.

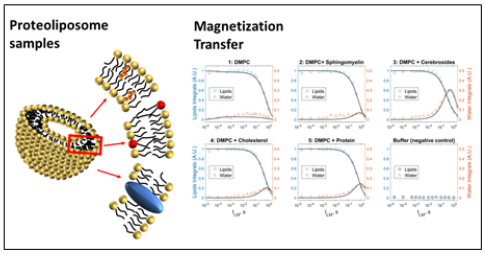

Magnetization Transfer in Proteoliposome Samples that Mimic the Protein and Lipid Composition of Myelin

Weiqi Yang, Jae-Seung Lee, Maureen Leninger, Johannes Windschuh, Nathaniel J. Traaseth and Alexej Jerschow*

Graphic Abstract

254x76mm (96 x 96 DPI)

Magnetization Transfer in Liposome and Proteoliposome Samples that Mimic the Protein and Lipid Composition of Myelin

Weiqi Yang[1], Jae-Seung Lee[1,2], Maureen Leninger[1], Johannes Windschuh[2], Nathaniel J. Traaseth[1] and Alexej Jerschow[1*]

[1]Department of Chemistry, New York University, New York, NY, United States

[2]Department of Radiology, New York University Langone Medical Center, New York, NY, United States

Key Words: Magnetization Transfer, Chemical Exchange Saturation Transfer, White matter diseases

Running Head: Magnetization Transfer in Proteolipisome Samples

* Corresponding Author

Alexej Jerschow: alexej.jerschow@nyu.edu

List of Abbreviations

DDM	*n*-Dodecyl β-D-Maltoside
DMPC	1,2-Dimyristoyl-*sn*-glycero-3-Phosphocholine
DQ	Double Quantum
DQF	Double-Quantum Filter
MBP	Myelin Basic Protein
MS	Multiple Sclerosis
MT	Magnetization Transfer
NOE	Nuclear Overhauser Effect
PLP	Proteolipid Protein
ZQ	Zero Quantum

ABSTRACT:

Although magnetization transfer (MT) was widely used in the brain MR imaging, such as brain inflammation and multiple sclerosis (MS), the detailed molecular origin of MT effects and the role of protein played in MT remain unclear. In this work, a proteoliposome model system was used to mimic the myelin environment and to examine the roles of protein, cholesterol, brain cerebrosides, and sphingomyelin embedded in the liposome matrix. Exchange parameters were determined using a double-quantum filter (DQF) experiment. The emphasis was on determining the relative contributions to exchange and magnetization transfer of cerebrosides, sphingomyelin, cholesterol, and protein in 1,2-dimyristoyl-*sn*-glycero-3-phosphocholine (DMPC) bilayers. The main finding is that cerebrosides, produce the strongest exchange effects, and that these were even more pronounced than those found for proteins. Sphingomyelin, which also has exchangeable groups at the head of the fatty acid chains, albeit closer to the lipid acyl chains, and cholesterol showed only minimal transfer. Overall, the extracted exchange rates appear much smaller than what is commonly assumed for –OH and –NH groups.

Introduction

Magnetization transfer (MT) has become a powerful and popular technique for imparting image contrast based on chemical exchange or cross-relaxation in macromolecular assemblies, especially for use in brain MRI. This contrast has been shown to produce indicators for certain abnormalities including brain inflammation and multiple sclerosis (MS).[1-4] In MT discussed here, the longitudinal magnetization of rigid or semisolid-like tissue is partially saturated and transferred to the free water pool. Residual dipolar couplings are responsible for the communication of the saturation levels towards the exchange site, which in turn transmits it to water. There are two generally accepted mechanisms for the transmission of saturation levels to the water pool: (a) chemical exchange and (b) cross relaxation through relayed nuclear Overhauser effect (NOE), with the latter often being very weak or non-existent.[5-7] MT contrast allows quantifying the macromolecular pool fraction to a certain extent, and such quantities have been correlated with myelin content as well as water content change in myelin tissue.[4,8,9]

Myelin is a multilayered stack of membranes consisting of 80% lipids by dry weight. The wrapping of multiple layers of myelin membrane sheets around an axon is of fundamental importance for the function of the nervous system. The lipids within myelin are composed of glycosphingomyelin (~27%), cholesterol (~44%), plasmalogens (~16%), and other phospholipids (sphingomyelin, phosphatidylinositol, phosphatidylserine, etc).[10,11] The protein-to-lipid ratio by weight is lower in myelin (~0.25), compared to a plasma membrane (from 1 to

0.25). There are generally two types of proteins in the myelin structure: the proteolipid protein (PLP) and myelin basic protein (MBP). PLP is a transmembrane protein which plays a role in the adhesion of the extracellular leaflets of the myelin membrane. MBP is a peripheral membrane protein which helps bring myelin bilayers close together by a combination of electrostatic and hydrophobic forces.[10] It has been demonstrated that one can directly image the short T_2 signal component in myelin using ultra-short TE imaging methods.[11] For human in vivo applications, such short echo times are typically unattainable. MT contrast provides an alternative, which, through repeated chemical exchange, leads to contrast enhancement for the detection of myelin. The mechanism of MT is of interest, because it may be relevant for the interpretation of imaging results and may allow the extraction of specific information on myelin composition and its environment.

Previous work examined the detailed molecular origin of MT contrast. Fralix *et al.* suggested that cholesterol was a key component for the generation of MT in lipid systems.[12] Kucharczyk *et al.* examined MT in synthetic lipids and concluded that galacto-cerebroside components had the largest contribution to MT.[13] Lee *et al.* and Malyarenko et al. identified that exchangeable groups were essential for effective MT, through experiments with a liquid crystal system,[14,15] thus direct NOE from macromolecules to water could be ruled out as the primary contrast mechanisms.[16,17] The quantitative magnetization transfer and the super-Lorentzian model were also used to detect the abnormality in human brains,[2,18-20] but MT research on multilamellar lipid phases was limited. The contribution of

cholesterol and protein concentration in modulating the MT effect remain unclear to date. Here, we investigated the detailed molecular origin of MT effects by using a liposome and proteoliposome model system containing 1,2-dimyristoyl-*sn*-glycero-3-phosphocholine (DMPC) and a 44 kDa membrane protein with transmembrane and extra-membrane portions to mimic the white matter system.[13,21] The liposome model system used here had multilamellar phases, which display orientational averaging – similar to what one would find in the brain in voxels where a distribution of orientations was found. The protein system we chose (fusion of EmrE[22] and maltose binding protein) shares strong resemblance to myelin basic protein, both in terms of the size of the soluble protein and the number of transmembrane domains of the membrane spanning region of myelin basic protein. We also examined the roles of cholesterol, brain cerebrosides, and sphingomyelin embedded in the liposome due to their large amounts of myelin and relatively large numbers of labile protons.[11] A double-quantum filter experiment[17] is shown to be particularly useful for extracting transfer parameters. Although myelin tissue is more complex than the samples considered here, we were aiming to reduce the complexity and confine the study to the investigation of the differential effects between different liposome components. The results may be valuable for the ultimate understanding of magnetization transfer processes in myelin tissue.

Theoretical Background

A Z-spectrum is commonly used to study the MT effect for a certain spin system.[15,21,23,24] It represents the collection of the water signals after presaturation at different frequency offsets, normalized to the signal without any presaturation.[25] This approach has certain limitations. For example, in a Z-spectrum it is very difficult to separate the exchange rates from the pool sizes in such measurements and also the contributions of the different components to the signal if a sizable macromolecular signal is present.[26] In this study, we hence chose another approach to tag the macromolecular pool using a double-quantum filtered MT (DQF-MT) experiment.[17] Upon selecting the semi-solid signal, one can follow the buildup of magnetization in the water pool resulting from the exchange with the macromolecular pool with this sequence.

This DQF-MT sequence was previously established as a method to examine exchange processes in a collagen-water system[17] The differentiation between the pools is established by the generation of double-quantum (DQ) coherences in the macromolecular pool due to residual dipolar couplings. Following an exchange period, one can track the dynamics of the exchange process originating from the macromolecules,[17] In this way, it was possible to separate the macromolecule from bulk water and therefore monitor its MT process.

The DQF-MT sequence used in this study is shown in Fig. 1. Key functions of the sequence[17] are described here for convenience. Following the initial 90° pulse, the second rank tensors $T_{2,\pm1}$ are generated during the first $\tau/2$ period. The second 90° pulse converts these to DQ coherence, which are

selectively filtered by a phase cycle. The third 90° pulse converts the filtered tensors $T_{2,\pm2}$ to $T_{2,\pm1}$, which evolve into $T_{1,\pm1}$ during the second $\tau/2$ period. After the fourth 90° pulse, the zero-quantum (ZQ) coherence $T_{1,0}$ is selectively filtered by a phase cycle and a subsequent waiting period t_{LM} allows for exchange. Following this exchange period, the last 90° pulse excites the single-quantum coherence for detection.

The combination of the DQ and ZQ filters are implemented by a 16-steps phase cycle: φ1 = (0 90° 180° 270° 90° 180° 270° 0 180° 270° 0 90° 270° 0 90° 180°), φ2= (0 0 0 0 90° 90° 90° 90° 180° 180° 180° 180° 270° 270° 270° 270°, φ3=0, φ_R= (180°, 0), instead of the 64-steps phase cycle presented in Ref.[17] We tested both phase cycling schemes and chose the former because it performed better in terms of filtering out the free water signal and saving experiment time. The first two RF pulses were grouped to select the DQ coherences. The third and fourth RF pulses were grouped to select the ZQ coherences.

During the exchange period t_{LM}, the evolution of the ZQ coherences may be described using chemical exchange and cross relaxation models.[17,27,28] The heterogeneous biological system can be treated as a two-phase proton system. The water and liposome protons constitute the two phases, and they are denoted by subscripts *w* and *l*, respectively. A common spin temperature will be rapidly established within the liposome and water phases by spin diffusion and magnetization transfer and by rapid chemical exchange between different environments, respectively.[27,28] This assumption can be justified on the basis of

the relative sizes of the dipolar couplings along the lipid chain. It was shown that the following equations could describe the exchange process during the period t_{LM}:[17,28]

$$M_{zl} = m_{zl}(t_{LM}t = 0)\left(a_+ e^{-tt_{LM}/T_{1+}} + a_- e^{-t_{LM}t/T_{1-}}\right) + m_{zw}(t_{LM}t = 0)b(e^{-t_{LM}t/T_{1-}} - e^{-t_{LM}t/T_{1+}})$$

$$M_{zw} = m_{zl}(t_{LM}t = 0)\frac{p_w}{p_l}b\left(e^{-t_{LM}t/T_{1-}} - e^{-t_{LM}t/T_{1+}}\right) + m_{zw}(t_{LM}t = 0)\left(a_- e^{-t_{LM}t/T_{1+}} + a_+ e^{-t_{LM}t/T_{1-}}\right)$$

$$a_\pm = \frac{1}{2}\left[1 \pm \frac{R_{1l} - R_{1w} + k - 2p_l k}{\sqrt{(R_{1l} - R_{1w} + k)^2 - 4p_l k(R_{1l} - R_{1w})}}\right]$$

$$b = \frac{p_l k}{\sqrt{(R_{1l} - R_{1w} + k)^2 - 4p_l k(R_{1l} - R_{1w})}}$$

$$\frac{1}{T_{1\pm}} = \frac{1}{2}\left[R_{1l} + R_{1w} + k \pm \sqrt{(R_{1l} + R_{1w} + k)^2 - 4p_l k(R_{1l} - R_{1w})}\right], \quad (1)$$

where ~~M_{zl},~~ m_{zl} ($t_{LM}t$ = 0), ~~M_{zw},~~ and m_{zw} ($t_{LM}t$ = 0) are the longitudinal magnetizations M_{zl} and M_{zw} for liposomes and water at $t_{LM}t$ = 0, respectively. R_{1l} and R_{1w} are the longitudinal relaxation rates for liposomes and water. p_l and p_w represent the fractions of the protons involved in the exchange process residing on the liposomes and water. The exchange rate, k, is the sum of the forward and backward reactions rates. When t_{LM} is zero or close to zero, chemical exchange has not developed yet, and we can assume m_{zw} ($t_{LM}t$ = 0) = 0. For a normalized signal strength, we can assume m_{zl} ($t_{LM}t$ = 0) = 1. Equation (1) becomes:

$$M_{zl} = \left(a_+ e^{-t_{LM}t/T_{1+}} + a_- e^{-t_{LM}t/T_{1-}}\right)$$

$$M_{zw} = \frac{p_w}{p_l} b\left(e^{-t_{LM}t/T_{1-}} - e^{-t_{LM}t/T_{1+}}\right)$$

$$a_\pm = \frac{1}{2}\left[1 \pm \frac{R_{1l} - R_{1w} + k - 2p_l k}{\sqrt{(R_{1l} - R_{1w} + k)^2 - 4p_l k(R_{1l} - R_{1w})}}\right]$$

$$b = \frac{p_l k}{\sqrt{(R_{1l} - R_{1w} + k)^2 - 4p_l k(R_{1l} - R_{1w})}}$$

$$\frac{1}{T_{1\pm}} = \frac{1}{2}[R_{1l} + R_{1w} + k \pm \sqrt{(R_{1l} + R_{1w} + k)^2 - 4p_l k(R_{1l} - R_{1w})}] \quad (2)$$

The exchange process between the lipids and water was dominated by the exchange rate *k*, the longitudinal relaxation rate for lipids and water, and the proton ratio between the fractions of the protons involved in the MT process.

Materials and Methods

Sample preparation

Fig. 2 shows the schematic of liposomes used for measurements of MT in a system designed to mimic multilamellar phase structure in white matter, which display similar orientational averaging. Please note that the samples couldn't not truly mimic white matter because of tissue complexity. The primary component of the liposomes was DMPC. Four additional components were included with the goal of delineating the MT mechanisms: cholesterol, sphingomyelin,

cerebrosides, and a fusion protein consisting of maltose binding protein and EmrE. Note that in the samples to assess the mechanisms of MT, the liposomes were prepared in multilamellar phases.

Liposome samples were prepared by dissolving DMPC (Avanti Polar Lipids, Inc., MW = 677.93 g/mol) in a 3:1 mixture of chloroform:methanol and dried under nitrogen gas to a thin film. To remove residual solvent, the film was dried overnight under vacuum.[29,30]

Sphingomyelin (extract from porcine brain, Avanti Polar Lipids, Inc., MW = 760.33 g/mol), cholesterol (Sigma-Aldrich, MW = 386.65 g/mol), or cerebrosides (brain extract from porcine; Avanti Polar Lipids, Inc., MW = 781.95 g/mol) were co-dissolved with DMPC at a 10% w/w concentration. The mixture was co-dissolved in a 3:1 mixture of chloroform:methanol, dried under nitrogen gas to a thin film, and lyophilized overnight. [29,30]

The samples with protein contained a fusion construct with maltose binding protein adjoined to EmrE. Maltose binding protein (globular) was positioned at the N-terminal side of the fusion construct, while EmrE (transmembrane) was at the C-terminal end. To reconstitute the protein into liposomes, the thin film of DMPC was rehydrated in 100 mM Na_2HPO_4 (pH = 7.0), 20 mM NaCl, and *n*-dodecyl β-D-maltoside (DDM) solubilized fusion protein. Samples were incubated overnight with Bio-Beads (Bio-Rad) to remove the detergent. The liposomes were pelleted at 300,000 x g for 2 h at 8 °C using a TLA-110 rotor (Beckman-Coulter). [29,30]

All samples were resuspended in 100 mM Na_2HPO_4, 20 mM NaCl at a pH of 7.0 and subjected to ten freeze/thaw cycles. The final composition was 300 µL buffer, 30 mg DMPC and 3 mg of the respective additive (sphingomyelin, cholesterol, cerebrosides or protein), as summarized in Table 1. The liposome suspensions were placed in a 5 mm o.d. NMR tube for subsequent spectroscopic measurements. [29,30]

NMR data acquisition

All experiments were performed on a Bruker Avance I spectrometer (Bruker, MA, USA) operating at 400.13 MHz for ^{1}H. The duration of the 90° pulse was 5.3 μs. The longitudinal T_1 relaxation times were measured for liposome samples using the inversion recovery experiment with a recovery delay of 20 s. All the experiments were done at room temperature (19 °C). Then, the recovery delays for individual samples were adjusted to be 5 times the corresponding T_{1w} values shown in Table 1.

Z-spectra under single RF irradiations and DQF spectra were obtained from each liposome sample. The Z-spectra were obtained with a 5 s-long continuous wave (cw) presaturation pulse followed by a 90° readout pulse. The amplitude ($\gamma B_1/2\pi$) of the presaturartion pulse was 500 Hz for all samples. Four transients were recorded for each frequency offset from -40,000 Hz to 40,000 Hz. The delay between each scan TR was 5 times the corresponding T_{1w} values shown in Table 1. The RF frequency offset for the Z-spectrum measurement was

(-120000 Hz, -40000 Hz, -36000 Hz, -32000 Hz, -28000 Hz, -24000 Hz, -22000 Hz, -20000 Hz, -18000 Hz, -16000 Hz, -14000 Hz, -12000 Hz, -10000 Hz, -8000 Hz, -6000 Hz, -5000 Hz, -4000 Hz, -3000 Hz, -2000 Hz, -1000 Hz, -800 Hz, -400 Hz, -200 Hz, 0, 200 Hz, 400 Hz, 800 Hz, 1000 Hz, 2000 Hz, 3000 Hz, 4000 Hz, 5000 Hz, 6000 Hz, 8000 Hz, 10000 Hz, 12000 Hz, 14000 Hz, 16000 Hz, 18000 Hz, 20000 Hz, 22000 Hz, 24000 Hz, 28000 Hz, 32000 Hz, 36000 Hz, 40000 Hz, 120000 Hz).

DQF spectra were obtained by the DQF-MT sequence given as a function of $\tau/2$ with $t_{LM} = t_{DQ} = 2$ μs. The number of averages for each scan were 16, which corresponded to one complete phase cycle, as shown in in Fig. 1. DQF spectra were obtained as a function of t_{LM} with $\tau/2 = 15$ μs. The τ delay was first optimized by observing the maximum DQ excitation. The τ delays ranged from 2 to 180 µs. As seen in Fig. S1, the broad lipid peak was strongest when $\tau/2 = 15$ µs. As shown in Fig. S2-S6, subsequent DQF experiments were performed with fixed $\tau/2 = 15$ µs and variable 14 to 16 exchange times t_{LM}, ranging from 20 µs to 1 s. The number of scans for each experiment was 128, which corresponded to repeating the whole phase cycle by 8 times. The delay t_{DQ} was 2 µs.

Data Processing

For each Z-spectrum, we integrated the water peak from -400 Hz to 400 Hz.

For each DQF spectrum, we integrated the 1D spectrum from -100 Hz to 200 Hz and from -25 kHz to 20 kHz. We assigned the first integral to water and the difference between two integrals to lipids. All the curves were normalized by the maximum of each curve. The non-linear least squares algorithm was used to fit the DQF data into Eq. (2). The relaxation term R_{1w} was constrained as the measured value, and R_{1l} was constrained within the range from 0 to 20 s^{-1}, since their values did not affect the fitting significantly. ~~Theoretically~~In principle, the sum of p_l and p_w should be 1 for an ideal two-site exchange system. ~~However, besides the additive lipids and protein~~The observed lipid signal, however, contains ~~, the lipid signal observed inevitably contained~~ the signal from DMPC, which will influence the results. Furthermore, the initial signal normalization can deviate from ideal behavior due to pulse sequence imperfections or relaxation effects during delays. Therefore, we fitted the DQF spectra without constraining $p_l + p_w = 1$ here. ~~We also ran the fitting with such constraint, and the result was shown in the supplemental information. Two results were very similar to each other.~~The fitting parameters are shown in Table 2. We also performed the fitting with the constraint for comparison (Fig. S7 and Table S1). The trends in the two types of analyses ~~Two results were~~ are very similar to each other. The smaller the fraction of the exchangeable species, the smaller the p_w values obtained, but the extracted exchange rates typically stay the same.

All the data processing and curve fittings were performed in Matlab R2014b (MathWorks, Natick, Massachusetts, USA). The functions *lsqcurvefit* and *nlparci* were used in the curve fitting.

Results and Discussion

The results from the DQF-MT experiments are presented in Fig. 3. For each sample, the water (blue circles) and lipids signals (orange triangles) are plotted against t_{LM}, together with the curves fitted to Eq. (2). All the liposome samples displayed buildups of the water signals. Such a buildup of the water signal does not exist in a pure buffer solution without any liposomes (control), as shown at the bottom rightmost panel of Fig. 3. The sample containing cerebrosides manifested the highest buildup of the water signal. Then, the samples containing protein and cholesterol follow, and the remaining two samples displayed similar maximum heights for buildups of the water signals. The decays of the lipids signals seem similar across the samples except the sample containing cerebrosides, in which the lipids signal decayed faster.

The fitted parameters for the DQF data to the model outlined in the Theory section are summarized in Table 2. The low p_w values of the sample contain DMPC was corresponding to the fact that the DMPC had no exchangeable proton in its molecular structure. Comparing the samples with cerebrosides and protein, the fitted parameters suggest that their p_w values might be similar, and the MT effects differ due to the exchange rate. The reason why the MT effect in the sample with cholesterol is smaller than in the samples containing cerebrosides and protein might be related to its smaller p_w, i.e. reduced water access. For the sample containing sphingomyelin, note that likewise the p_w

values are relatively low, indicating that water access is much lower than to the sugar entities of cerebrosides.

Proton exchanges between lipids and free water are influenced by several factors such as the number of exchangeable groups in lipids, the pH of the sample relative to pertinent pK_a values, and the accessibility of the exchangeable groups to free water. In DMPC, the phosphate group is deprotonated at the pH of the buffer solution used in this work and was expected to have reduced MT effects as observed in experimental data. Sphingomyelin contains one hydroxyl and one amide groups, which may be responsible for its MT effect. Cholesterol has only one hydroxyl group but produces a stronger MT effect than sphingomyelin, which is likely due to its smaller molecular weight and thus greater number of moles per weight present since liposome samples were prepared at a constant 10% weight incorporation. Finally, cerebrosides have four hydroxyl groups residing on the hydrophilic head, corresponding to its strongest MT effect.

Proteins have several exchangeable protons present at the backbone and side chain residues. The fitted results shown in Table 2 suggest that the accessibility to free water was similar between protein and cerebrosides liposome samples, which is intuitive. The lower exchange rate for protein is surprising nonetheless, resulting in a lower amount of MT relative to cerebroside samples. Fig. S7 shows Z-spectra of all these samples, roughly indicating the relative trends observed here. It is more difficult to extract similar data from Z-spectra since one cannot cleanly separate the pools. The DQF spectrum

provides the opportunity to select the lipid component specifically at the start of each exchange period.

Conclusion

In this work, exchange parameters have been determined in samples mimicking myelin composition. The emphasis was on determining the relative contributions to exchange and magnetization transfer of cerebrosides, sphingomyelin, cholesterol, and protein in DMPC bilayers. A DQF-MT experiment was used to determine exchange rates and relative (accessible) pool sizes. The main finding is that cerebrosides, produced the strongest exchange effects, and that these were even more pronounced than those found for proteins. Sphingomyelin, which also has exchangeable groups at the head of the fatty acid chains, albeit closer to the lipid acyl chains, showed only minimal transfer. The same was found for cholesterol as well. These results could help in identifying MT contrast in white matter. Overall, the extracted exchange rates appear much smaller than what is commonly assumed for –OH and –NH groups.

Acknowledgements

This work was supported in part by the National Institutes of Health (R01EB016045 to A.J.; R01AI108889 to N.J.T), and in part by the US National Science Foundation (NSF CHE 1710046 to A.J.).

References:

1. Liu Z, Pardini M, Yaldizli O, et al. Magnetization transfer ratio measures in normal-appearing white matter show periventricular gradient abnormalities in multiple sclerosis. *Brain.* 2015;138(Pt 5):1239-1246.
2. Harrison NA, Cooper E, Dowell NG, et al. Quantitative Magnetization Transfer Imaging as a Biomarker for Effects of Systemic Inflammation on the Brain. *Biol Psychiatry.* 2015;78(1):49-57.
3. Janve VA, Zu Z, Yao SY, et al. The radial diffusivity and magnetization transfer pool size ratio are sensitive markers for demyelination in a rat model of type III multiple sclerosis (MS) lesions. *Neuroimage.* 2013;74:298-305.
4. Schmierer K, Scaravilli F, Altmann DR, Barker GJ, Miller DH. Magnetization transfer ratio and myelin in postmortem multiple sclerosis brain. *Ann Neurol.* 2004;56(3):407-415.
5. Jones CK, Huang A, Xu J, et al. Nuclear Overhauser enhancement (NOE) imaging in the human brain at 7T. *Neuroimage.* 2013;77:114-124.
6. Jones CK, Polders D, Hua J, et al. In vivo three-dimensional whole-brain pulsed steady-state chemical exchange saturation transfer at 7 T. *Magn Reson Med.* 2012;67(6):1579-1589.
7. Ling W, Regatte RR, Navon G, Jerschow A. Assessment of glycosaminoglycan concentration in vivo by chemical exchange-dependent saturation transfer (gagCEST). *Proc Natl Acad Sci U S A.* 2008;105(7):2266-2270.
8. Gass A, Barker GJ, Kidd D, et al. Correlation of magnetization transfer ratio with clinical disability in multiple sclerosis. *Ann Neurol.* 1994;36(1):62-67.
9. Vavasour IM, Laule C, Li DK, Traboulsee AL, MacKay AL. Is the magnetization transfer ratio a marker for myelin in multiple sclerosis? *J Magn Reson Imaging.* 2011;33(3):713-718.
10. Aggarwal S, Yurlova L, Simons M. Central nervous system myelin: structure, synthesis and assembly. *Trends Cell Biol.* 2011;21(10):585-593.

11. Wilhelm MJ, Ong HH, Wehrli SL, et al. Direct magnetic resonance detection of myelin and prospects for quantitative imaging of myelin density. *Proc Natl Acad Sci U S A.* 2012;109(24):9605-9610.
12. Fralix TA, Ceckler TL, Wolff SD, Simon SA, Balaban RS. Lipid bilayer and water proton magnetization transfer: effect of cholesterol. *Magn Reson Med.* 1991;18(1):214-223.
13. Kucharczyk W, Macdonald PM, Stanisz GJ, Henkelman RM. Relaxivity and magnetization transfer of white matter lipids at MR imaging: importance of cerebrosides and pH. *Radiology.* 1994;192(2):521-529.
14. Malyarenko DI, Zimmermann EM, Adler J, Swanson SD. Magnetization transfer in lamellar liquid crystals. *Magn Reson Med.* 2014;72(5):1427-1434.
15. Lee JS, Regatte, R. R., Jerschow, A. Magnetization transfer in a partly deuterated lyotropic liquid crystal by single- and dual-frequency RF irradiations. *Journal of Magnetic Resonance.* 2017;281:141-150.
16. van Zijl PC, Zhou J, Mori N, Payen JF, Wilson D, Mori S. Mechanism of magnetization transfer during on-resonance water saturation. A new approach to detect mobile proteins, peptides, and lipids. *Magn Reson Med.* 2003;49(3):440-449.
17. Eliav U, Navon G. Multiple quantum filtered NMR studies of the interaction between collagen and water in the tendon. *J Am Chem Soc.* 2002;124(12):3125-3132.
18. Zaiss M, Bachert P. Chemical exchange saturation transfer (CEST) and MR Z-spectroscopy in vivo: a review of theoretical approaches and methods. *Phys Med Biol.* 2013;58(22):R221-269.
19. Ge Y, Grossman RI, Babb JS, Rabin ML, Mannon LJ, Kolson DL. Age-related total gray matter and white matter changes in normal adult brain. Part II: quantitative magnetization transfer ratio histogram analysis. *AJNR Am J Neuroradiol.* 2002;23(8):1334-1341.
20. Morrison C, Henkelman RM. A model for magnetization transfer in tissues. *Magn Reson Med.* 1995;33(4):475-482.
21. Swanson SD, Malyarenko DI, Fabiilli ML, Welsh RC, Nielsen JF, Srinivasan A. Molecular, dynamic, and structural origin of inhomogeneous magnetization transfer in lipid membranes. *Magn Reson Med.* 2017;77(3):1318-1328.
22. UniProt. https://www.uniprot.org/uniprot/P23895. Accessed.
23. Xu X, Yadav NN, Zeng H, et al. Magnetization transfer contrast-suppressed imaging of amide proton transfer and relayed nuclear overhauser enhancement chemical exchange saturation transfer effects in the human brain at 7T. *Magn Reson Med.* 2016;75(1):88-96.
24. Lee JS, Parasoglou P, Xia D, Jerschow A, Regatte RR. Uniform magnetization transfer in chemical exchange saturation transfer magnetic resonance imaging. *Sci Rep.* 2013;3:1707.
25. van Ziji PCM, Yadav, Nirbhay N. Chemical Exchange Saturation Transfer (CEST): what is in a name and what isn't? *Magn Reson Med.* 2011;65(4):927-948.
26. Zaiss M, Schmitt B, Bachert P. Quantitative separation of CEST effect from magnetization transfer and spillover effects by Lorentzian-line-fit analysis of z-spectra. *J Magn Reson.* 2011;211(2):149-155.
27. Edzes HT, Samson RS. The Measurement of Cross-Relaxation Effects in the Proton NMR Spin-Lattice of Water in Biological Systems: Hydrated Collagen and Muscle. *J Magn Reson.* 1978;31:207-229.
28. Edzes HT, Samulski ET. Cross relaxation and spin diffusion in the proton NMR or hydrated collagen. *Nature.* 1977;265(5594):521-523.

29. Gayen A, Banigan JR, Traaseth NJ. Ligand-induced conformational changes of the multidrug resistance transporter EmrE probed by oriented solid-state NMR spectroscopy. *Angew Chem Int Ed Engl.* 2013;52(39):10321-10324.
30. Gayen A, Leninger M, Traaseth NJ. Protonation of a glutamate residue modulates the dynamics of the drug transporter EmrE. *Nat Chem Biol.* 2016;12(3):141-145.

Table 1 The longitudinal relaxation time for water (w) and lipids (l) of each liposome sample measured using an inversion recovery experiment.

Samples number	1	2	3	4	5
Composition	DMPC	DMPC + sphingomyelin	DMPC + cerebrosides	DMPC + cholesterol	DMPC + protein
R_{1w} (s^{-1})	0.46	0.48	0.52	0.41	0.43
R_{1l}(s^{-1})	7.14	6.25	7.14	2.13	1.72

Table 2 Magnetization transfer rates *k* and other parameters for five liposome samples by DQF spectrum fitting

Number	Sample	R_{1w} (s^{-1}) (fixed)	R_{1l}(s^{-1}) (constrained)	*k* (s^{-1}) (with confidence interval)	p_w	p_l
1	DMPC	0.46	1.52 (1.43, 1.60)	484 (-8, 977)	0.06	1
2	DMPC + sphingomyelin	0.48	1.58 (1.40, 1.76)	269.40 (-191, 730)	0.06	1
3	DMPC + cerebrosides	0.52	1.48 (1.09, 1.87)	2.89 (2.10, 3.68)	0.69	0.57
4	DMPC + cholesterol	0.41	1.72 (0.23, 3.20)	1.67 (-1.31, 4.66)	0.33	1
5	DMPC + protein	0.43	1.35 (-1.75, 4.45)	0.78 (-2.19, 3.76)	0.63	0.62

Magnetization Transfer in Liposome and Proteoliposome Samples that Mimic the Protein and Lipid Composition of Myelin

Weiqi Yang[1], Jae-Seung Lee[1,2], Maureen Leninger[1], Johannes Windschuh[2], Nathaniel J. Traaseth[1] and Alexej Jerschow[1*]

[1]Department of Chemistry, New York University, New York, NY, United States

[2]Department of Radiology, New York University Langone Medical Center, New York, NY, United States

Key Words: Magnetization Transfer, Chemical Exchange Saturation Transfer, White matter diseases

Running Head: Magnetization Transfer in Proteolipisome Samples

* Corresponding Author

Alexej Jerschow: alexej.jerschow@nyu.edu

List of Abbreviations

DDM	*n*-Dodecyl β-D-Maltoside
DMPC	1,2-Dimyristoyl-*sn*-glycero-3-Phosphocholine
DQ	Double Quantum
DQF	Double-Quantum Filter
MBP	Myelin Basic Protein
MS	Multiple Sclerosis
MT	Magnetization Transfer
NOE	Nuclear Overhauser Effect
PLP	Proteolipid Protein
ZQ	Zero Quantum

ABSTRACT:

Although magnetization transfer (MT) was widely used in the brain MR imaging, such as brain inflammation and multiple sclerosis (MS), the detailed molecular origin of MT effects and the role of protein played in MT remain unclear. In this work, a proteoliposome model system was used to mimic the myelin environment and to examine the roles of protein, cholesterol, brain cerebrosides, and sphingomyelin embedded in the liposome matrix. Exchange parameters were determined using a double-quantum filter (DQF) experiment. The emphasis was on determining the relative contributions to exchange and magnetization transfer of cerebrosides, sphingomyelin, cholesterol, and protein in 1,2-dimyristoyl-*sn*-glycero-3-phosphocholine (DMPC) bilayers. The main finding is that cerebrosides, produce the strongest exchange effects, and that these were even more pronounced than those found for proteins. Sphingomyelin, which also has exchangeable groups at the head of the fatty acid chains, albeit closer to the lipid acyl chains, and cholesterol showed only minimal transfer. Overall, the extracted exchange rates appear much smaller than what is commonly assumed for –OH and –NH groups.

Introduction

Magnetization transfer (MT) has become a powerful and popular technique for imparting image contrast based on chemical exchange or cross-relaxation in macromolecular assemblies, especially for use in brain MRI. This contrast has been shown to produce indicators for certain abnormalities including brain inflammation and multiple sclerosis (MS).[1-4] In MT discussed here, the longitudinal magnetization of rigid or semisolid-like tissue is partially saturated and transferred to the free water pool. Residual dipolar couplings are responsible for the communication of the saturation levels towards the exchange site, which in turn transmits it to water. There are two generally accepted mechanisms for the transmission of saturation levels to the water pool: (a) chemical exchange and (b) cross relaxation through relayed nuclear Overhauser effect (NOE), with the latter often being very weak or non-existent.[5-7] MT contrast allows quantifying the macromolecular pool fraction to a certain extent, and such quantities have been correlated with myelin content as well as water content change in myelin tissue.[4,8,9]

Myelin is a multilayered stack of membranes consisting of 80% lipids by dry weight. The wrapping of multiple layers of myelin membrane sheets around an axon is of fundamental importance for the function of the nervous system. The lipids within myelin are composed of glycosphingomyelin (~27%), cholesterol (~44%), plasmalogens (~16%), and other phospholipids (sphingomyelin, phosphatidylinositol, phosphatidylserine, etc).[10,11] The protein-to-lipid ratio by weight is lower in myelin (~0.25), compared to a plasma membrane (from 1 to

0.25). There are generally two types of proteins in the myelin structure: the proteolipid protein (PLP) and myelin basic protein (MBP). PLP is a transmembrane protein which plays a role in the adhesion of the extracellular leaflets of the myelin membrane. MBP is a peripheral membrane protein which helps bring myelin bilayers close together by a combination of electrostatic and hydrophobic forces.[10] It has been demonstrated that one can directly image the short T_2 signal component in myelin using ultra-short TE imaging methods.[11] For human in vivo applications, such short echo times are typically unattainable. MT contrast provides an alternative, which, through repeated chemical exchange, leads to contrast enhancement for the detection of myelin. The mechanism of MT is of interest, because it may be relevant for the interpretation of imaging results and may allow the extraction of specific information on myelin composition and its environment.

Previous work examined the detailed molecular origin of MT contrast. Fralix *et al.* suggested that cholesterol was a key component for the generation of MT in lipid systems.[12] Kucharczyk *et al.* examined MT in synthetic lipids and concluded that galacto-cerebroside components had the largest contribution to MT.[13] Lee *et al.* and Malyarenko et al. identified that exchangeable groups were essential for effective MT, through experiments with a liquid crystal system,[14,15] thus direct NOE from macromolecules to water could be ruled out as the primary contrast mechanisms.[16,17] The quantitative magnetization transfer and the super-Lorentzian model were also used to detect the abnormality in human brains,[2,18-20] but MT research on multilamellar lipid phases was limited. The contribution of

cholesterol and protein concentration in modulating the MT effect remain unclear to date. Here, we investigated the detailed molecular origin of MT effects by using a liposome and proteoliposome model system containing 1,2-dimyristoyl-*sn*-glycero-3-phosphocholine (DMPC) and a 44 kDa membrane protein with transmembrane and extra-membrane portions to mimic the white matter system.[13,21] The liposome model system used here had multilamellar phases, which display orientational averaging – similar to what one would find in the brain in voxels where a distribution of orientations was found. The protein system we chose (fusion of EmrE[22] and maltose binding protein) shares strong resemblance to myelin basic protein, both in terms of the size of the soluble protein and the number of transmembrane domains of the membrane spanning region of myelin basic protein. We also examined the roles of cholesterol, brain cerebrosides, and sphingomyelin embedded in the liposome due to their large amounts of myelin and relatively large numbers of labile protons.[11] A double-quantum filter experiment[17] is shown to be particularly useful for extracting transfer parameters. Although myelin tissue is more complex than the samples considered here, we were aiming to reduce the complexity and confine the study to the investigation of the differential effects between different liposome components. The results may be valuable for the ultimate understanding of magnetization transfer processes in myelin tissue.

Theoretical Background

A Z-spectrum is commonly used to study the MT effect for a certain spin system.[15,21,23,24] It represents the collection of the water signals after presaturation at different frequency offsets, normalized to the signal without any presaturation.[25] This approach has certain limitations. For example, in a Z-spectrum it is very difficult to separate the exchange rates from the pool sizes in such measurements and also the contributions of the different components to the signal if a sizable macromolecular signal is present.[26] In this study, we hence chose another approach to tag the macromolecular pool using a double-quantum filtered MT (DQF-MT) experiment.[17] Upon selecting the semi-solid signal, one can follow the buildup of magnetization in the water pool resulting from the exchange with the macromolecular pool with this sequence.

This DQF-MT sequence was previously established as a method to examine exchange processes in a collagen-water system[17] The differentiation between the pools is established by the generation of double-quantum (DQ) coherences in the macromolecular pool due to residual dipolar couplings. Following an exchange period, one can track the dynamics of the exchange process originating from the macromolecules,[17] In this way, it was possible to separate the macromolecule from bulk water and therefore monitor its MT process.

The DQF-MT sequence used in this study is shown in Fig. 1. Key functions of the sequence[17] are described here for convenience. Following the initial 90° pulse, the second rank tensors $T_{2,\pm1}$ are generated during the first $\tau/2$ period. The second 90° pulse converts these to DQ coherence, which are

selectively filtered by a phase cycle. The third 90° pulse converts the filtered tensors $T_{2,\pm2}$ to $T_{2,\pm1}$, which evolve into $T_{1,\pm1}$ during the second $\tau/2$ period. After the fourth 90° pulse, the zero-quantum (ZQ) coherence $T_{1,0}$ is selectively filtered by a phase cycle and a subsequent waiting period t_{LM} allows for exchange. Following this exchange period, the last 90° pulse excites the single-quantum coherence for detection.

The combination of the DQ and ZQ filters are implemented by a 16-steps phase cycle: φ1 = (0 90° 180° 270° 90° 180° 270° 0 180° 270° 0 90° 270° 0 90° 180°), φ2= (0 0 0 0 90° 90° 90° 90° 180° 180° 180° 180° 270° 270° 270° 270°, φ3=0, φ_R= (180°, 0), instead of the 64-steps phase cycle presented in Ref.[17] We tested both phase cycling schemes and chose the former because it performed better in terms of filtering out the free water signal and saving experiment time. The first two RF pulses were grouped to select the DQ coherences. The third and fourth RF pulses were grouped to select the ZQ coherences.

During the exchange period t_{LM}, the evolution of the ZQ coherences may be described using chemical exchange and cross relaxation models.[17,27,28] The heterogeneous biological system can be treated as a two-phase proton system. The water and liposome protons constitute the two phases, and they are denoted by subscripts *w* and *l*, respectively. A common spin temperature will be rapidly established within the liposome and water phases by spin diffusion and magnetization transfer and by rapid chemical exchange between different environments, respectively.[27,28] This assumption can be justified on the basis of

the relative sizes of the dipolar couplings along the lipid chain. It was shown that the following equations could describe the exchange process during the period t_{LM}:[17,28]

$$M_{zl} = m_{zl}(t_{LM}=0)\left(a_+ e^{-t_{LM}/T_{1+}} + a_- e^{-t_{LM}/T_{1-}}\right) + m_{zw}(t_{LM}=0)b(e^{-t_{LM}/T_{1-}} - e^{-t_{LM}/T_{1+}})$$

$$M_{zw} = m_{zl}(t_{LM}=0)\frac{p_w}{p_l}b\left(e^{-t_{LM}/T_{1-}} - e^{-t_{LM}/T_{1+}}\right) + m_{zw}(t_{LM}=0)\left(a_- e^{-t_{LM}/T_{1+}} + a_+ e^{-t_{LM}/T_{1-}}\right)$$

$$a_\pm = \frac{1}{2}\left[1 \pm \frac{R_{1l} - R_{1w} + k - 2p_l k}{\sqrt{(R_{1l} - R_{1w} + k)^2 - 4p_l k(R_{1l} - R_{1w})}}\right]$$

$$b = \frac{p_l k}{\sqrt{(R_{1l} - R_{1w} + k)^2 - 4p_l k(R_{1l} - R_{1w})}}$$

$$\frac{1}{T_{1\pm}} = \frac{1}{2}\left[R_{1l} + R_{1w} + k \pm \sqrt{(R_{1l} + R_{1w} + k)^2 - 4p_l k(R_{1l} - R_{1w})}\right], \quad (1)$$

where m_{zl} (t_{LM}= 0), and m_{zw} (t_{LM}= 0) are the longitudinal magnetizations M_{zl} and M_{zw} for liposomes and water at t_{LM}= 0, respectively. R_{1l} and R_{1w} are the longitudinal relaxation rates for liposomes and water. p_l and p_w represent the fractions of the protons involved in the exchange process residing on the liposomes and water. The exchange rate, k, is the sum of the forward and backward reactions rates. When t_{LM} is zero or close to zero, chemical exchange has not developed yet, and we can assume m_{zw} (t_{LM}= 0) = 0. For a normalized signal strength, we can assume m_{zl} (t_{LM}= 0) = 1. Equation (1) becomes:

$$M_{zl} = \left(a_+ e^{-t_{LM}/T_{1+}} + a_- e^{-t_{LM}/T_{1-}}\right)$$

$$M_{zw} = \frac{p_w}{p_l} b\left(e^{-t_{LM}/T_{1-}} - e^{-t_{LM}/T_{1+}}\right)$$

$$a_\pm = \frac{1}{2}\left[1 \pm \frac{R_{1l} - R_{1w} + k - 2p_l k}{\sqrt{(R_{1l} - R_{1w} + k)^2 - 4p_l k(R_{1l} - R_{1w})}}\right]$$

$$b = \frac{p_l k}{\sqrt{(R_{1l} - R_{1w} + k)^2 - 4p_l k(R_{1l} - R_{1w})}}$$

$$\frac{1}{T_{1\pm}} = \frac{1}{2}[R_{1l} + R_{1w} + k \pm \sqrt{(R_{1l} + R_{1w} + k)^2 - 4p_l k(R_{1l} - R_{1w})}] \quad (2)$$

The exchange process between the lipids and water was dominated by the exchange rate *k*, the longitudinal relaxation rate for lipids and water, and the proton ratio between the fractions of the protons involved in the MT process.

Materials and Methods

Sample preparation

Fig. 2 shows the schematic of liposomes used for measurements of MT in a system designed to mimic multilamellar phase structure in white matter, which display similar orientational averaging. Please note that the samples couldn't not truly mimic white matter because of tissue complexity. The primary component of the liposomes was DMPC. Four additional components were included with the goal of delineating the MT mechanisms: cholesterol, sphingomyelin,

cerebrosides, and a fusion protein consisting of maltose binding protein and EmrE. Note that in the samples to assess the mechanisms of MT, the liposomes were prepared in multilamellar phases.

Liposome samples were prepared by dissolving DMPC (Avanti Polar Lipids, Inc., MW = 677.93 g/mol) in a 3:1 mixture of chloroform:methanol and dried under nitrogen gas to a thin film. To remove residual solvent, the film was dried overnight under vacuum.[29,30]

Sphingomyelin (extract from porcine brain, Avanti Polar Lipids, Inc., MW = 760.33 g/mol), cholesterol (Sigma-Aldrich, MW = 386.65 g/mol), or cerebrosides (brain extract from porcine; Avanti Polar Lipids, Inc., MW = 781.95 g/mol) were co-dissolved with DMPC at a 10% w/w concentration. The mixture was co-dissolved in a 3:1 mixture of chloroform:methanol, dried under nitrogen gas to a thin film, and lyophilized overnight. [29,30]

The samples with protein contained a fusion construct with maltose binding protein adjoined to EmrE. Maltose binding protein (globular) was positioned at the N-terminal side of the fusion construct, while EmrE (transmembrane) was at the C-terminal end. To reconstitute the protein into liposomes, the thin film of DMPC was rehydrated in 100 mM Na_2HPO_4 (pH = 7.0), 20 mM NaCl, and *n*-dodecyl β-D-maltoside (DDM) solubilized fusion protein. Samples were incubated overnight with Bio-Beads (Bio-Rad) to remove the detergent. The liposomes were pelleted at 300,000 x g for 2 h at 8 °C using a TLA-110 rotor (Beckman-Coulter). [29,30]

All samples were resuspended in 100 mM Na_2HPO_4, 20 mM NaCl at a pH of 7.0 and subjected to ten freeze/thaw cycles. The final composition was 300 µL buffer, 30 mg DMPC and 3 mg of the respective additive (sphingomyelin, cholesterol, cerebrosides or protein), as summarized in Table 1. The liposome suspensions were placed in a 5 mm o.d. NMR tube for subsequent spectroscopic measurements. [29,30]

NMR data acquisition

All experiments were performed on a Bruker Avance I spectrometer (Bruker, MA, USA) operating at 400.13 MHz for ^{1}H. The duration of the 90° pulse was 5.3 μs. The longitudinal T_1 relaxation times were measured for liposome samples using the inversion recovery experiment with a recovery delay of 20 s. All the experiments were done at room temperature (19 °C). Then, the recovery delays for individual samples were adjusted to be 5 times the corresponding T_{1w} values shown in Table 1.

Z-spectra under single RF irradiations and DQF spectra were obtained from each liposome sample. The Z-spectra were obtained with a 5 s-long continuous wave (cw) presaturation pulse followed by a 90° readout pulse. The amplitude ($\gamma B_1/2\pi$) of the presaturartion pulse was 500 Hz for all samples. Four transients were recorded for each frequency offset from -40,000 Hz to 40,000 Hz. The delay between each scan TR was 5 times the corresponding T_{1w} values shown in Table 1. The RF frequency offset for the Z-spectrum measurement was

(-120000 Hz, -40000 Hz, -36000 Hz, -32000 Hz, -28000 Hz, -24000 Hz, -22000 Hz, -20000 Hz, -18000 Hz, -16000 Hz, -14000 Hz, -12000 Hz, -10000 Hz, -8000 Hz, -6000 Hz, -5000 Hz, -4000 Hz, -3000 Hz, -2000 Hz, -1000 Hz, -800 Hz, -400 Hz, -200 Hz, 0, 200 Hz, 400 Hz, 800 Hz, 1000 Hz, 2000 Hz, 3000 Hz, 4000 Hz, 5000 Hz, 6000 Hz, 8000 Hz, 10000 Hz, 12000 Hz, 14000 Hz, 16000 Hz, 18000 Hz, 20000 Hz, 22000 Hz, 24000 Hz, 28000 Hz, 32000 Hz, 36000 Hz, 40000 Hz, 120000 Hz).

DQF spectra were obtained by the DQF-MT sequence given as a function of $\tau/2$ with $t_{LM} = t_{DQ} = 2$ μs. The number of averages for each scan were 16, which corresponded to one complete phase cycle, as shown in in Fig. 1. DQF spectra were obtained as a function of t_{LM} with $\tau/2 = 15$ μs. The τ delay was first optimized by observing the maximum DQ excitation. The τ delays ranged from 2 to 180 µs. As seen in Fig. S1, the broad lipid peak was strongest when $\tau/2 = 15$ µs. As shown in Fig. S2-S6, subsequent DQF experiments were performed with fixed $\tau/2 = 15$ µs and variable 14 to 16 exchange times t_{LM}, ranging from 20 µs to 1 s. The number of scans for each experiment was 128, which corresponded to repeating the whole phase cycle by 8 times. The delay t_{DQ} was 2 µs.

Data Processing

For each Z-spectrum, we integrated the water peak from -400 Hz to 400 Hz.

For each DQF spectrum, we integrated the 1D spectrum from -100 Hz to 200 Hz and from -25 kHz to 20 kHz. We assigned the first integral to water and the difference between two integrals to lipids. All the curves were normalized by the maximum of each curve. The non-linear least squares algorithm was used to fit the DQF data into Eq. (2). The relaxation term R_{1w} was constrained as the measured value, and R_{1l} was constrained within the range from 0 to 20 s^{-1}, since their values did not affect the fitting significantly. In principle, the sum of p_l and p_w should be 1 for an ideal two-site exchange system. The observed lipid signal, however, contains the signal from DMPC, which will influence the results. Furthermore, the initial signal normalization can deviate from ideal behavior due to pulse sequence imperfections or relaxation effects during delays. Therefore, we fitted the DQF spectra without constraining $p_l + p_w = 1$ here. The fitting parameters are shown in Table 2. We also performed the fitting with the constraint for comparison (Fig. S7 and Table S1). The trends in the two types of analyses are very similar to each other. The smaller the fraction of the exchangeable species, the smaller the p_w values obtained, but the extracted exchange rates typically stay the same.

All the data processing and curve fittings were performed in Matlab R2014b (MathWorks, Natick, Massachusetts, USA). The functions *lsqcurvefit* and *nlparci* were used in the curve fitting.

Results and Discussion

The results from the DQF-MT experiments are presented in Fig. 3. For each sample, the water (blue circles) and lipids signals (orange triangles) are plotted against t_{LM}, together with the curves fitted to Eq. (2). All the liposome samples displayed buildups of the water signals. Such a buildup of the water signal does not exist in a pure buffer solution without any liposomes (control), as shown at the bottom rightmost panel of Fig. 3. The sample containing cerebrosides manifested the highest buildup of the water signal. Then, the samples containing protein and cholesterol follow, and the remaining two samples displayed similar maximum heights for buildups of the water signals. The decays of the lipids signals seem similar across the samples except the sample containing cerebrosides, in which the lipids signal decayed faster.

The fitted parameters for the DQF data to the model outlined in the Theory section are summarized in Table 2. The low p_w values of the sample contain DMPC was corresponding to the fact that the DMPC had no exchangeable proton in its molecular structure. Comparing the samples with cerebrosides and protein, the fitted parameters suggest that their p_w values might be similar, and the MT effects differ due to the exchange rate. The reason why the MT effect in the sample with cholesterol is smaller than in the samples containing cerebrosides and protein might be related to its smaller p_w, i.e. reduced water access. For the sample containing sphingomyelin, note that likewise the p_w values are relatively low, indicating that water access is much lower than to the sugar entities of cerebrosides.

Proton exchanges between lipids and free water are influenced by several factors such as the number of exchangeable groups in lipids, the pH of the sample relative to pertinent pK_a values, and the accessibility of the exchangeable groups to free water. In DMPC, the phosphate group is deprotonated at the pH of the buffer solution used in this work and was expected to have reduced MT effects as observed in experimental data. Sphingomyelin contains one hydroxyl and one amide groups, which may be responsible for its MT effect. Cholesterol has only one hydroxyl group but produces a stronger MT effect than sphingomyelin, which is likely due to its smaller molecular weight and thus greater number of moles per weight present since liposome samples were prepared at a constant 10% weight incorporation. Finally, cerebrosides have four hydroxyl groups residing on the hydrophilic head, corresponding to its strongest MT effect.

Proteins have several exchangeable protons present at the backbone and side chain residues. The fitted results shown in Table 2 suggest that the accessibility to free water was similar between protein and cerebrosides liposome samples, which is intuitive. The lower exchange rate for protein is surprising nonetheless, resulting in a lower amount of MT relative to cerebroside samples. Fig. S7 shows Z-spectra of all these samples, roughly indicating the relative trends observed here. It is more difficult to extract similar data from Z-spectra since one cannot cleanly separate the pools. The DQF spectrum provides the opportunity to select the lipid component specifically at the start of each exchange period.

Conclusion

In this work, exchange parameters have been determined in samples mimicking myelin composition. The emphasis was on determining the relative contributions to exchange and magnetization transfer of cerebrosides, sphingomyelin, cholesterol, and protein in DMPC bilayers. A DQF-MT experiment was used to determine exchange rates and relative (accessible) pool sizes. The main finding is that cerebrosides, produced the strongest exchange effects, and that these were even more pronounced than those found for proteins. Sphingomyelin, which also has exchangeable groups at the head of the fatty acid chains, albeit closer to the lipid acyl chains, showed only minimal transfer. The same was found for cholesterol as well. These results could help in identifying MT contrast in white matter. Overall, the extracted exchange rates appear much smaller than what is commonly assumed for –OH and –NH groups.

Acknowledgements

This work was supported in part by the National Institutes of Health (R01EB016045 to A.J.; R01AI108889 to N.J.T). The experiments were performed in the Shared Instrument Facility of the Department of Chemistry, New York University, supported by the US National Science Foundation under grant number CHE0116222.

References:

1. Liu Z, Pardini M, Yaldizli O, et al. Magnetization transfer ratio measures in normal-appearing white matter show periventricular gradient abnormalities in multiple sclerosis. *Brain.* 2015;138(Pt 5):1239-1246.
2. Harrison NA, Cooper E, Dowell NG, et al. Quantitative Magnetization Transfer Imaging as a Biomarker for Effects of Systemic Inflammation on the Brain. *Biol Psychiatry.* 2015;78(1):49-57.
3. Janve VA, Zu Z, Yao SY, et al. The radial diffusivity and magnetization transfer pool size ratio are sensitive markers for demyelination in a rat model of type III multiple sclerosis (MS) lesions. *Neuroimage.* 2013;74:298-305.
4. Schmierer K, Scaravilli F, Altmann DR, Barker GJ, Miller DH. Magnetization transfer ratio and myelin in postmortem multiple sclerosis brain. *Ann Neurol.* 2004;56(3):407-415.
5. Jones CK, Huang A, Xu J, et al. Nuclear Overhauser enhancement (NOE) imaging in the human brain at 7T. *Neuroimage.* 2013;77:114-124.
6. Jones CK, Polders D, Hua J, et al. In vivo three-dimensional whole-brain pulsed steady-state chemical exchange saturation transfer at 7 T. *Magn Reson Med.* 2012;67(6):1579-1589.
7. Ling W, Regatte RR, Navon G, Jerschow A. Assessment of glycosaminoglycan concentration in vivo by chemical exchange-dependent saturation transfer (gagCEST). *Proc Natl Acad Sci U S A.* 2008;105(7):2266-2270.
8. Gass A, Barker GJ, Kidd D, et al. Correlation of magnetization transfer ratio with clinical disability in multiple sclerosis. *Ann Neurol.* 1994;36(1):62-67.
9. Vavasour IM, Laule C, Li DK, Traboulsee AL, MacKay AL. Is the magnetization transfer ratio a marker for myelin in multiple sclerosis? *J Magn Reson Imaging.* 2011;33(3):713-718.
10. Aggarwal S, Yurlova L, Simons M. Central nervous system myelin: structure, synthesis and assembly. *Trends Cell Biol.* 2011;21(10):585-593.
11. Wilhelm MJ, Ong HH, Wehrli SL, et al. Direct magnetic resonance detection of myelin and prospects for quantitative imaging of myelin density. *Proc Natl Acad Sci U S A.* 2012;109(24):9605-9610.
12. Fralix TA, Ceckler TL, Wolff SD, Simon SA, Balaban RS. Lipid bilayer and water proton magnetization transfer: effect of cholesterol. *Magn Reson Med.* 1991;18(1):214-223.
13. Kucharczyk W, Macdonald PM, Stanisz GJ, Henkelman RM. Relaxivity and magnetization transfer of white matter lipids at MR imaging: importance of cerebrosides and pH. *Radiology.* 1994;192(2):521-529.

14. Malyarenko DI, Zimmermann EM, Adler J, Swanson SD. Magnetization transfer in lamellar liquid crystals. *Magn Reson Med.* 2014;72(5):1427-1434.
15. Lee JS, Regatte, R. R., Jerschow, A. Magnetization transfer in a partly deuterated lyotropic liquid crystal by single- and dual-frequency RF irradiations. *Journal of Magnetic Resonance.* 2017;281:141-150.
16. van Zijl PC, Zhou J, Mori N, Payen JF, Wilson D, Mori S. Mechanism of magnetization transfer during on-resonance water saturation. A new approach to detect mobile proteins, peptides, and lipids. *Magn Reson Med.* 2003;49(3):440-449.
17. Eliav U, Navon G. Multiple quantum filtered NMR studies of the interaction between collagen and water in the tendon. *J Am Chem Soc.* 2002;124(12):3125-3132.
18. Zaiss M, Bachert P. Chemical exchange saturation transfer (CEST) and MR Z-spectroscopy in vivo: a review of theoretical approaches and methods. *Phys Med Biol.* 2013;58(22):R221-269.
19. Ge Y, Grossman RI, Babb JS, Rabin ML, Mannon LJ, Kolson DL. Age-related total gray matter and white matter changes in normal adult brain. Part II: quantitative magnetization transfer ratio histogram analysis. *AJNR Am J Neuroradiol.* 2002;23(8):1334-1341.
20. Morrison C, Henkelman RM. A model for magnetization transfer in tissues. *Magn Reson Med.* 1995;33(4):475-482.
21. Swanson SD, Malyarenko DI, Fabiilli ML, Welsh RC, Nielsen JF, Srinivasan A. Molecular, dynamic, and structural origin of inhomogeneous magnetization transfer in lipid membranes. *Magn Reson Med.* 2017;77(3):1318-1328.
22. UniProt. https://www.uniprot.org/uniprot/P23895. Accessed.
23. Xu X, Yadav NN, Zeng H, et al. Magnetization transfer contrast-suppressed imaging of amide proton transfer and relayed nuclear overhauser enhancement chemical exchange saturation transfer effects in the human brain at 7T. *Magn Reson Med.* 2016;75(1):88-96.
24. Lee JS, Parasoglou P, Xia D, Jerschow A, Regatte RR. Uniform magnetization transfer in chemical exchange saturation transfer magnetic resonance imaging. *Sci Rep.* 2013;3:1707.
25. van Ziji PCM, Yadav, Nirbhay N. Chemical Exchange Saturation Transfer (CEST): what is in a name and what isn't? *Magn Reson Med.* 2011;65(4):927-948.
26. Zaiss M, Schmitt B, Bachert P. Quantitative separation of CEST effect from magnetization transfer and spillover effects by Lorentzian-line-fit analysis of z-spectra. *J Magn Reson.* 2011;211(2):149-155.
27. Edzes HT, Samson RS. The Measurement of Cross-Relaxation Effects in the Proton NMR Spin-Lattice of Water in Biological Systems: Hydrated Collagen and Muscle. *J Magn Reson.* 1978;31:207-229.
28. Edzes HT, Samulski ET. Cross relaxation and spin diffusion in the proton NMR or hydrated collagen. *Nature.* 1977;265(5594):521-523.
29. Gayen A, Banigan JR, Traaseth NJ. Ligand-induced conformational changes of the multidrug resistance transporter EmrE probed by oriented solid-state NMR spectroscopy. *Angew Chem Int Ed Engl.* 2013;52(39):10321-10324.
30. Gayen A, Leninger M, Traaseth NJ. Protonation of a glutamate residue modulates the dynamics of the drug transporter EmrE. *Nat Chem Biol.* 2016;12(3):141-145.

Table 1 The longitudinal relaxation time for water (w) and lipids (l) of each liposome sample measured using an inversion recovery experiment.

Samples number	1	2	3	4	5
Composition	DMPC	DMPC + sphingomyelin	DMPC + cerebrosides	DMPC + cholesterol	DMPC + protein
R_{1w} (s^{-1})	0.46	0.48	0.52	0.41	0.43
R_{1l}(s^{-1})	7.14	6.25	7.14	2.13	1.72

Table 2 Magnetization transfer rates *k* and other parameters for five liposome samples by DQF spectrum fitting

Number	Sample	R_{1w} (s^{-1}) (fixed)	R_{1l}(s^{-1}) (constrained)	*k* (s^{-1}) (with confidence interval)	p_w	p_l
1	DMPC	0.46	1.52 (1.43, 1.60)	484 (-8, 977)	0.06	1
2	DMPC + sphingomyelin	0.48	1.58 (1.40, 1.76)	269.40 (-191, 730)	0.06	1
3	DMPC + cerebrosides	0.52	1.48 (1.09, 1.87)	2.89 (2.10, 3.68)	0.69	0.57
4	DMPC + cholesterol	0.41	1.72 (0.23, 3.20)	1.67 (-1.31, 4.66)	0.33	1
5	DMPC + protein	0.43	1.35 (-1.75, 4.45)	0.78 (-2.19, 3.76)	0.63	0.62

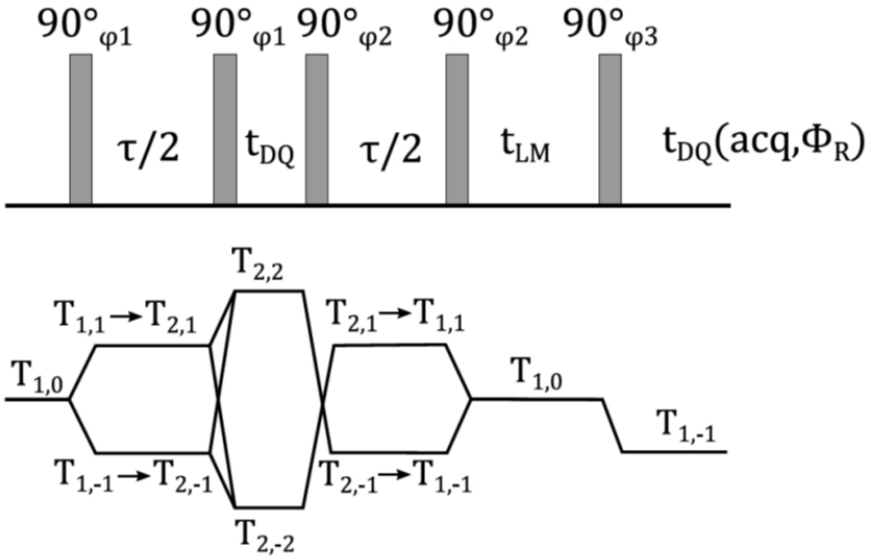

Fig.1 DQF-MT pulse sequence. A 16-steps phase cycling was used: φ1 = (0 90° 180° 270° 90° 180° 270° 0 180° 270° 0 90° 270° 0 90° 180°), φ2= (0 0 0 0 90° 90° 90° 90° 180° 180° 180° 180° 270° 270° 270° 270°, φ3=0, φR= (180°, 0).

254x190mm (96 x 96 DPI)

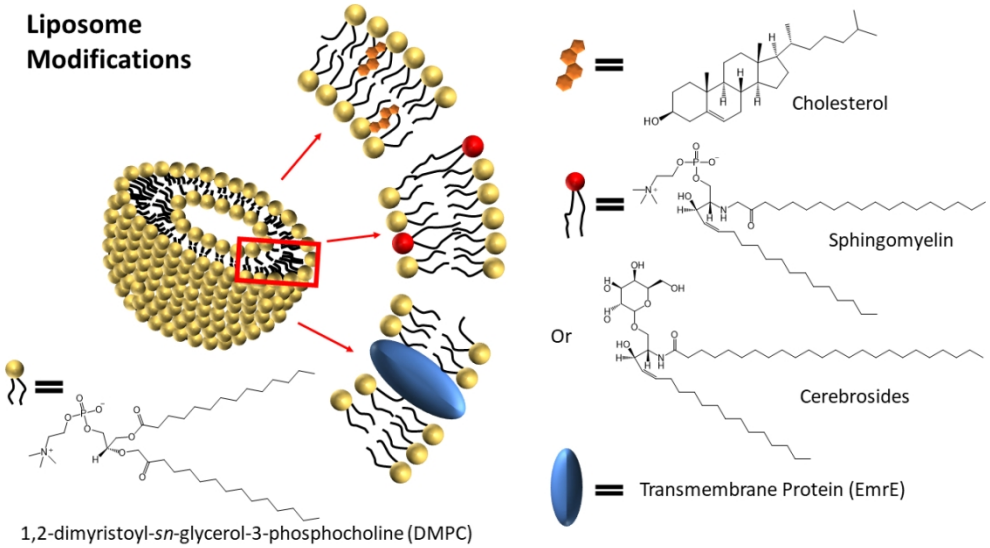

Fig. 2 Schematic of liposomes used for measurements of MT in a system designed to mimic white matter. The primary component of the liposomes was 1,2-dimyristoyl-sn-glycerol-3-phosphocholine (DMPC). Four additional components were included with the goal of delineating the MT mechanisms: cholesterol, sphingomyelin, cerebrosides, and a fusion protein consisting of maltose binding protein and EmrE. The chemical structures of sphingomyelin and cerebrosides were representative structures since a lipid extract would display a range of possible lipids lengths and saturation levels. Note that in the samples were prepared in multilamellar phases.

338x190mm (96 x 96 DPI)

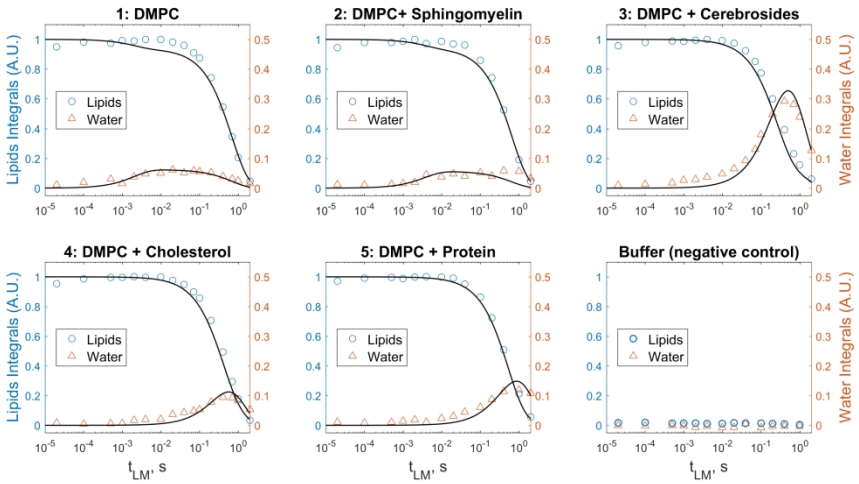

Fig. 3 DQF-MT integrals for water and lipids shown in separate panels for each sample as a function of tLM. The blue circle data point represents the integral of lipids, corresponding to the left blue y-axis. The orange triangle represents the integral of water, corresponding to the right orange y-axis. The control experiment is shown in the bottom right panel and represented the negative control for this set of experiments. Data were fitted using equation (1) (solid lines) with the parameters given in Table 3.

714x357mm (96 x 96 DPI)

Supplementary Information

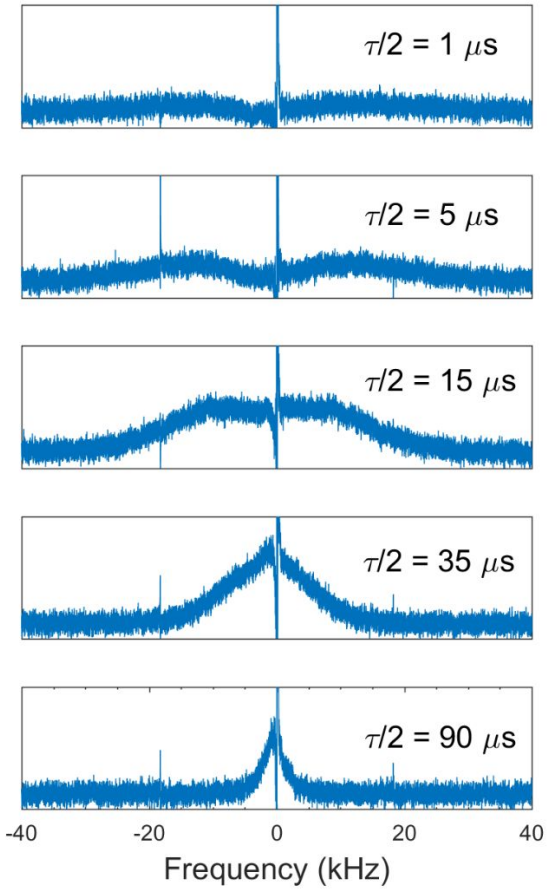

Fig. S1 Spectra obtained using the DQF pulse sequence in Fig. 1, given as a function of $\tau/2$ with $t_{LM} = t_{DQ}$=2 μs for the liposome sample composed of DMPC and cerebrosides. The spectra for other liposome samples gave a similar profile.

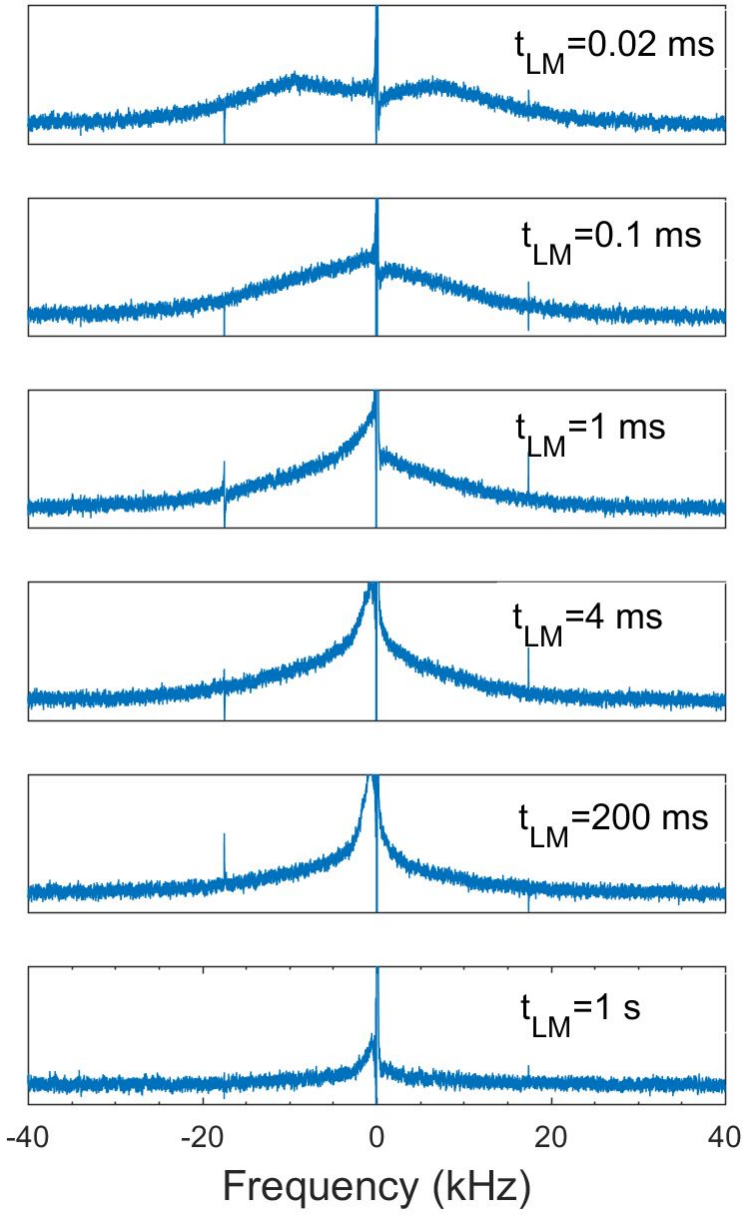

Fig. S2 Representative DQF spectra obtained by the DQF pulse sequence for various t_{LM} with $\tau/2$= 15 μs for liposomes solution contained DMPC only.

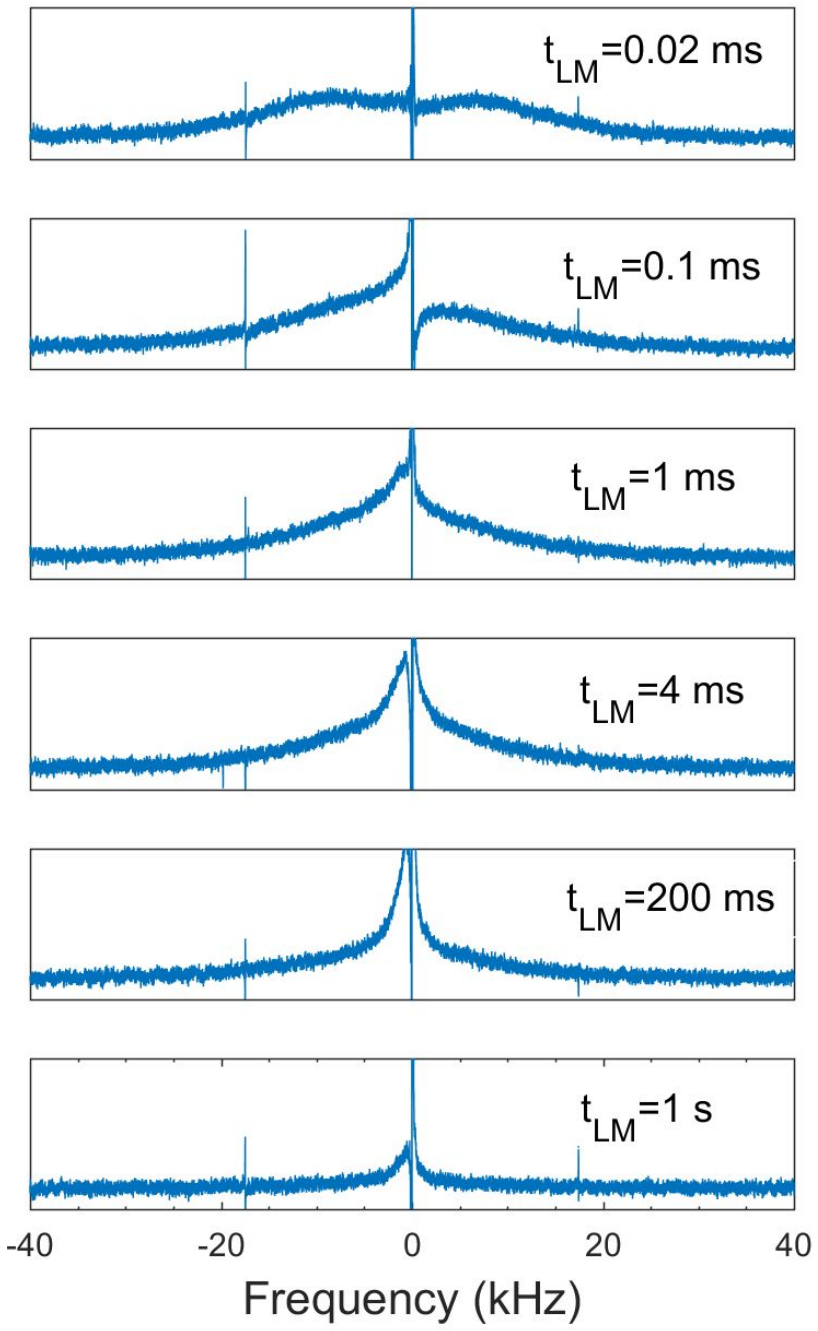

Fig. S3 Representative DQF spectra obtained by the DQF pulse sequence for various t_{LM} with $\tau/2$= 15 μs for liposomes solution contained DMPC and sphingomyelin.

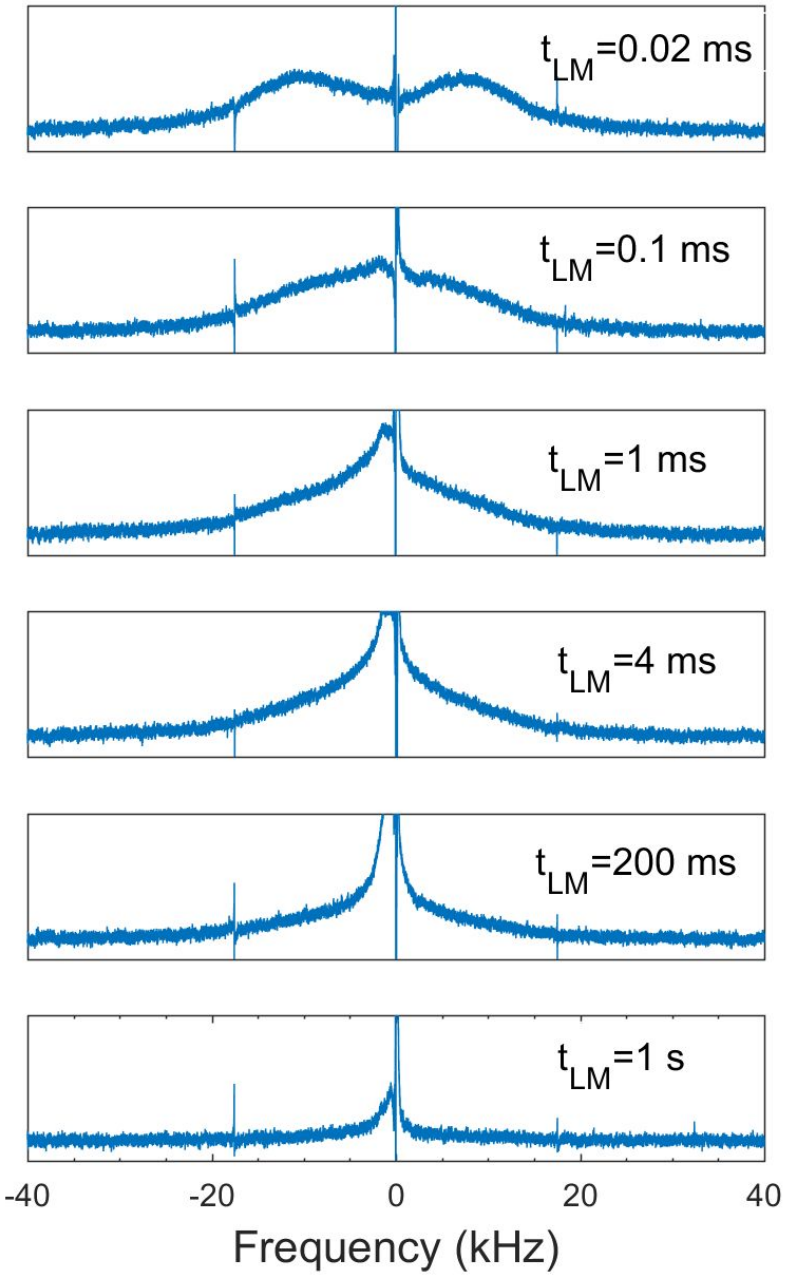

Fig. S4 Representative DQF spectra obtained by the DQF pulse sequence for various t_{LM} with $\tau/2$= 15 μs for liposomes solution contained DMPC and cholesterol.

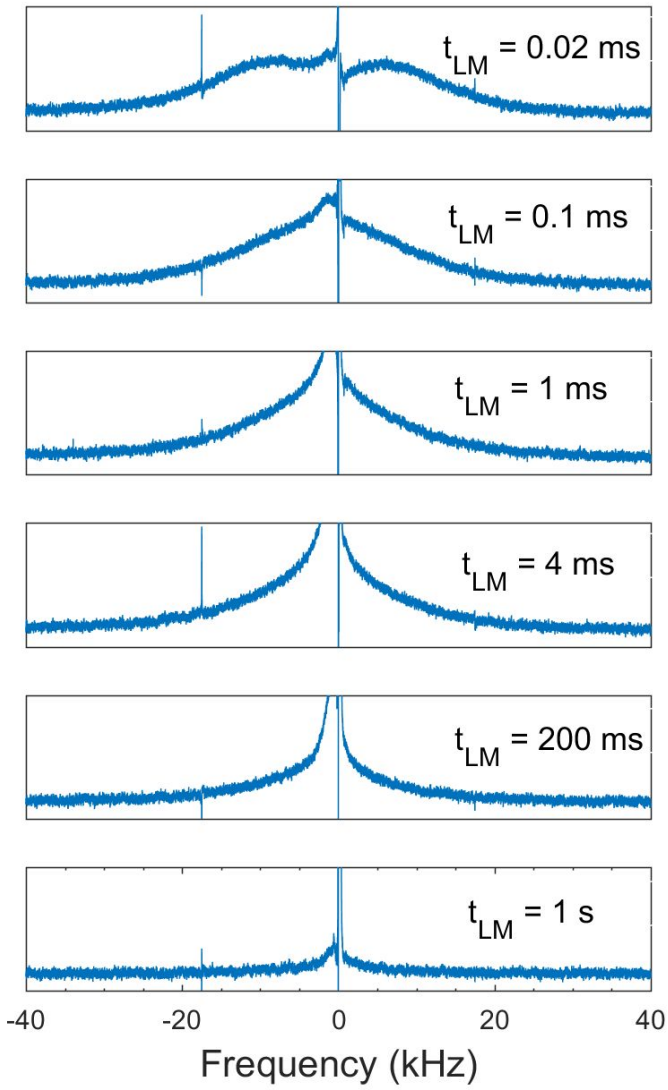

Fig. S5 Representative DQF spectra obtained by the DQF pulse sequence for various t_{LM} with $\tau/2$= 15 μs for liposomes solution contained DMPC and cerebrosides.

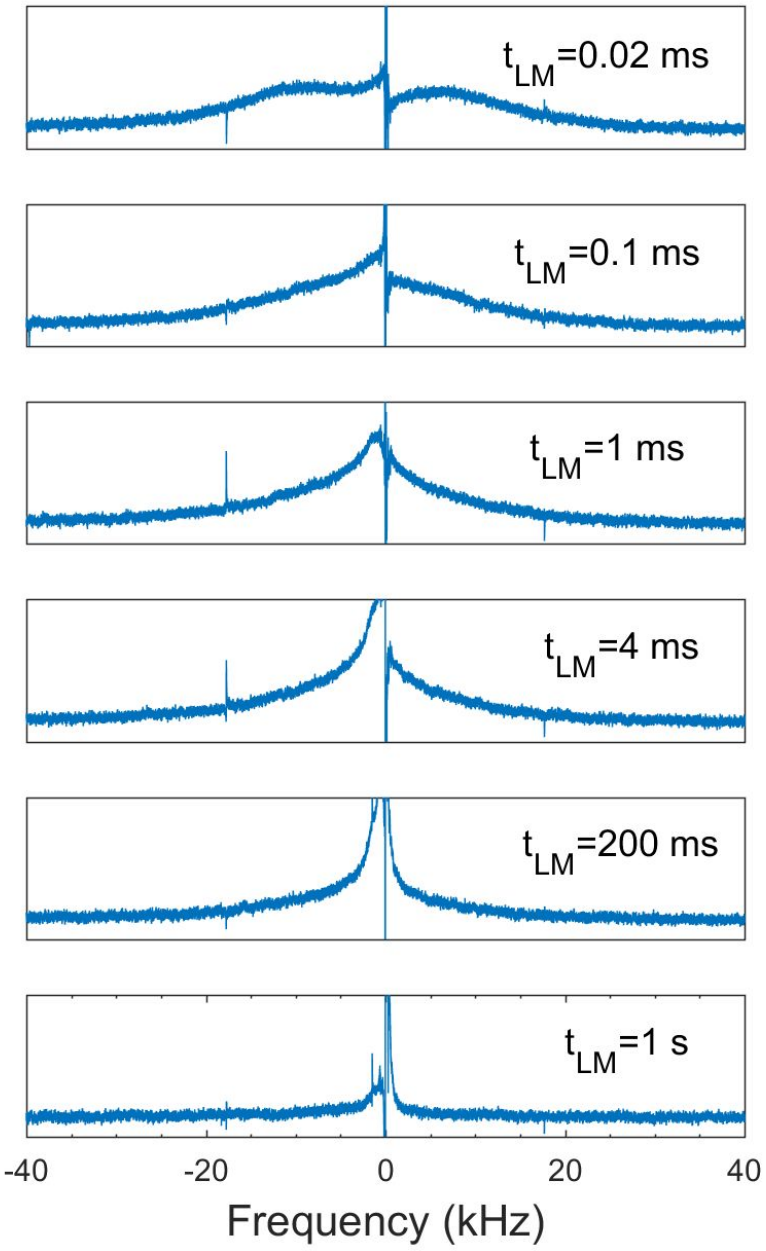

Fig. S6 Representative DQF spectra obtained by the DQF pulse sequence for various t_{LM} with $\tau/2$= 15 μs for liposomes solution contained DMPC and protein.

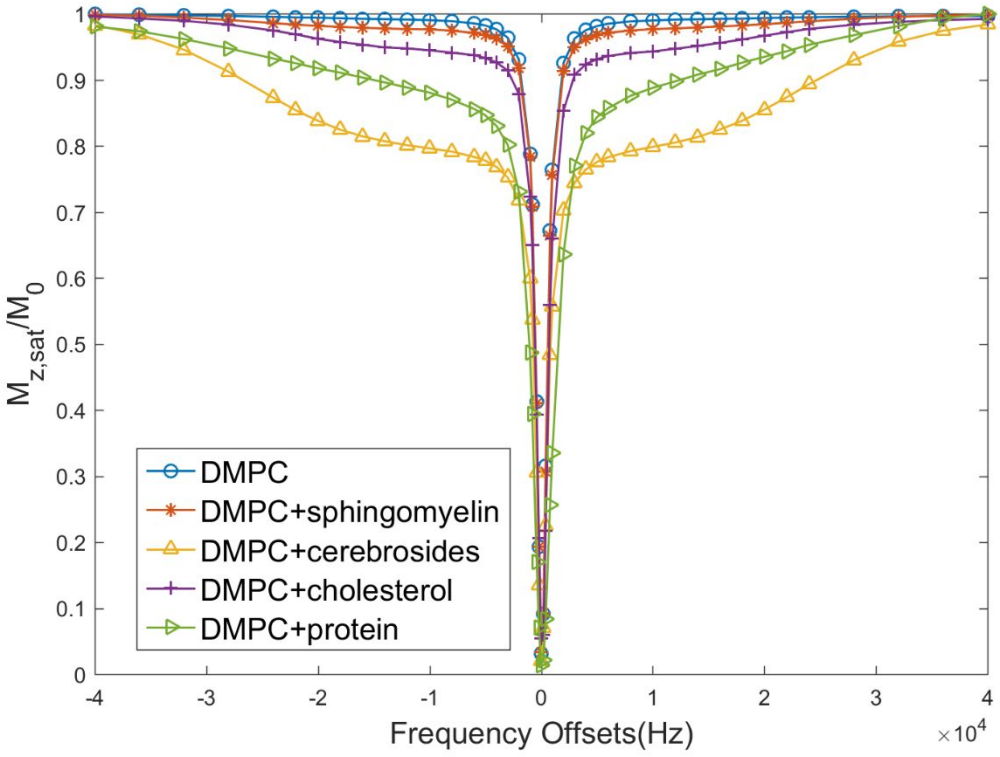

Fig. S7 Z-spectra for each liposomes samples, acquired with a 5 s-long continuous wave pulse with amplitude ($\gamma B_1/2\pi$) of 500 Hz.

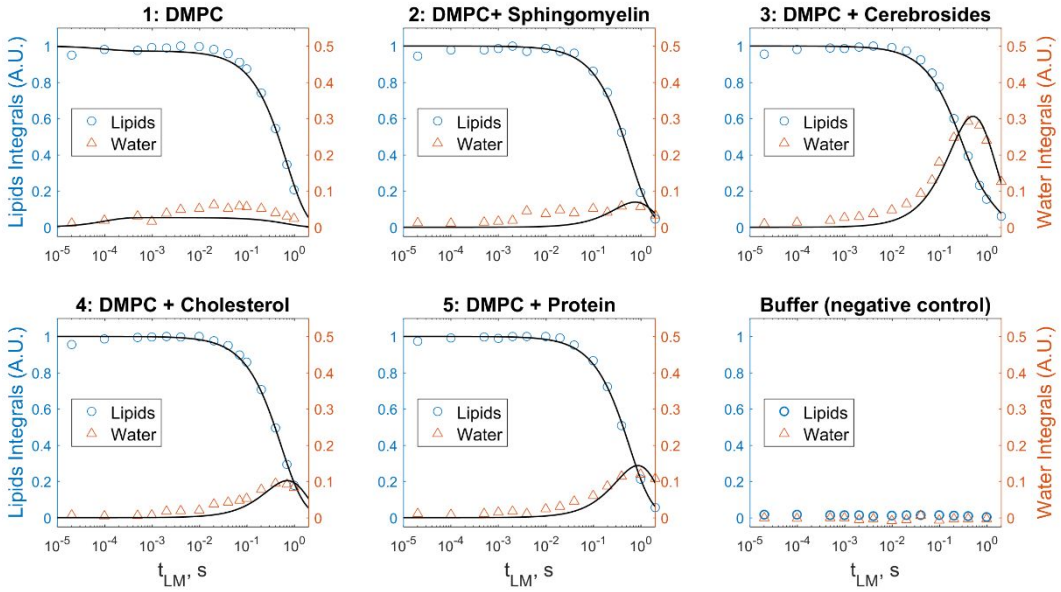

Fig. S8 DQF-MT integrals for water and lipids shown in separate panels for each sample as a function of t_{LM}. The blue circle data point represents the integral of lipids, corresponding to the left blue y-axis. The orange triangle represents the integral of water, corresponding to the right orange y-axis. The control experiment is shown in the bottom right panel and represented the negative control for this set of experiments. Data were fitted using equation (1) (solid lines) with constraining $p_w + p_l = 1$. The parameters were given in Table S1.

Table S1 Magnetization transfer rates *k* and other parameters for five liposome samples [a]

Number	Sample	R_{1w} (s^{-1})	R_{1l} (s^{-1})	*k* (s^{-1}) (with confidence interval)	p_w (with confidence interval)
1	DMPC	0.46	1.47	10000 (-26239, 46239)	0.027 (0.013, 0.040)
2	DMPC + sphingomyelin	0.48	1.40 (1.14, 1.66)	0.85 (-0.59, 2.29)	0.30 (-0.05, 0.65)
3	DMPC + cerebrosides	0.52	1.10 (0.88, 1.32)	3.17 (2.43, 3.92)	0.57 (0.51, 0.63)
4	DMPC + cholesterol	0.41	1.43 (0.93, 1.93)	1.14 (0.29, 1.99)	0.35 (0.12, 0.58)
5	DMPC + protein	0.43	1.20 (-0.36, 2.76)	0.87 (-0.81, 2.56)	0.54 (0.35, 0.73)

a: The rate *k* represents the magnetization transfer rate, which contained the influence of chemical exchange and relayed NOE; The proton ratios p_w were the fractions of exchangeable protons residing in water, with constraining $p_w + p_l = 1$.